Supporting Information

Smith et al. 10.1073/pnas.0905267106

SI Text

BrainMap Activation Experiment Data and Analysis. The BrainMap database contains the results of a large number of brain activation studies; at the time of our analyses, it contained the results from 1,687 journal articles. Each study can involve multiple "conditions," for example, comparing finger tapping with rest and comparing different rates of tapping with each other. The 1,687 studies resulted in 7,342 separate activation images and between them involved 29,671 human subjects. In the BrainMap database, the spatial distributions of these activations are represented via the coordinate locations of statistically-significant local maxima in the activation images. All coordinates are in a standard brain "space," in the case of BrainMap, the Talairach coordinate system (1). For each activation result, we recreated a 2-mm-resolution standard space pseudoactivation image by filling an empty image with points corresponding to the activation coordinates and then convolving this with a Gaussian kernel of FWHM 12 mm (2). Although the actual spatial extent of the original activation has not been preserved, this smoothing extent is a reasonably close match to that applied as data preprocessing in most FMRI activation studies and is close to the spatial variability in database coordinate locations as carefully investigated by ref. 3. We tested other spatial smoothing extents from 8- to 15-mm FWHM and found the results not significantly sensitive to the exact extent.

The resulting 7,342 activation images are concatenated together to produce a 2D dataset, where the first dimension is space (the 3 spatial dimensions are "unwrapped" onto 1 dimension), and the second is experiment ID (1:7,342; this dimension is referred to as "time" at points in our text, as a convenient shorthand, and in analogy to the temporal dimension in the resting FMRI data). For the PCA-based dimensionality reduction (described below) it is necessary for the data to be demeaned; also, as part of the pre-ICA processing, all voxels' time series are normalized to have variance of unity. These 2 practical data transformations are necessary in order for the PCA and ICA models to function correctly but do result in the presence of a few "artifactual" components in the ICA output. For parts of standard space involving very few nonzero values in the raw data (e.g., in voxels that do not correspond to gray matter), the combination of demeaning (of what was originally positive or zero data) and the variance normalization of voxels' time series (poorly conditioned and inflated in such voxels) leads to meaningless components. These can be seen below in *Results: 20-Dimensional Results in Detail* and are easily identified and discarded from further consideration.

The initial spatial maps generated by the principal component analysis (run before the final ICA) are not generally interpretable; although they "span the space" of the strongest d covariance components in the database, they are uninterpretably separated from each other because of the mathematical constraint in PCA that components are orthogonal in space and time. ICA aims to resolve this problem, by optimizing the independence of the resulting spatial maps while applying only a weak constraint on the relationship between any 2 networks' associated time courses; in ICA, time courses only have to be noncolinear, just as is required for the covariates in a multiple regression. Indeed, ICA resembles multiple regression, being different in that the covariates here are estimated from the data. In effect, the ICA "unmixing" is applying the central limit theorem in reverse, utilizing the fact that the optimal (and most meaningful) identification of components is achieved by minimizing the mutual statistical dependence between any 2 estimated components. A further strength of an ICA decomposition is that the ICA model allows any given brain region to be associated with >1 component, if the region's time series is a linear combination of the time series of >1 component. This makes biological sense, because a given point in the brain may be part of >1 functional network, but in general, such a representation is not possible with many other (e.g., clustering-based) approaches to multivariate decompositions. Hence, we apply ICA to identify the primary "independent components" in this data: d spatial maps, each with its own associated experiment ID time course that describes how strongly that particular map was relevant to each of the original 7,342 activation maps.

For the ICA decomposition, we used the MELODIC (multivariate exploratory linear optimized decomposition into independent components) tool (4) in the FSL [FMRIB Software Library (5, 6)] brain image analysis tool set. The ICA spatial maps are scaled by dividing by the noise standard deviation image from the residuals of the initial PCA-based dimensionality estimation and then Gaussianized by fitting a Gaussian-center γ-tailed mixture model, with the parameters of the fitted "null" Gaussian used to set the background mode to zero and background standard deviation to unity. The final ICA spatial maps were affine-transformed from BrainMap standard space (Talairach space) into 2-mm MNI152 space. These maps are, at any given dimensionality d, the $d - n_{\text{artifacts}}$ most representative functional networks from the entire BrainMap database.

Resting FMRI Experiment Data and Analysis. The resting-state FMRI dataset and analysis followed a fairly standard protocol, albeit with a higher number of subjects than often acquired for resting state experiments. Thirty-six healthy adult subjects were imaged (age range = 20–35 y, mean = 28.5 y; 21 male, 15 female) in a 3T Siemens Trio MRI scanner, using a 12-channel head coil. Structural brain images were acquired by using a T1-weighted 3D MPRAGE sequence with whole-head coverage, TR = 2.04 s, TE = 4.7 ms, flip angle = 8°, resolution $1 \times 1 \times 1$ mm, total acquisition time 12 min. These were used purely to aid the registration of the functional data into a common standard brain coordinate system (MNI152). Resting FMRI BOLD (blood oxygenation level-dependent) data were acquired with a standard gradient echo echo-planar-imaging (EPI) acquisition, TR = 2 s, TE = 28 ms, flip angle = 89°, resolution $3 \times 3 \times 3.5$ mm, whole-head coverage except for the lowest parts of the cerebellum in some subjects. The resting FMRI scan lasted 6 min. Ambient light was minimized, and the subjects were instructed to lie with eyes open, think of nothing in particular, and not to fall asleep. This dataset is not related to any experiments contained in BrainMap.

Data preprocessing was carried out with FSL tools. The following prestatistics processing was applied for each subject: head motion correction by using MCFLIRT (7); non-brain-removal by using BET (8); spatial smoothing by using a Gaussian kernel of FWHM 5 mm; grand-mean intensity normalization of the entire 4D dataset by a single multiplicative factor; high-pass temporal filtering (subtraction of Gaussian-weighted least-squares straight-line fitting, with $\sigma = 50.0$ s). Registration of each subject's FMRI data to that subject's high-resolution structural image was carried out by using FLIRT (7). Registration from the high-resolution structurals to MNI152 standard space was achieved by using FLIRT affine registration and then further refined by using FNIRT nonlinear registration (9, 10).

All subjects' 4D FMRI time series data were transformed into standard space at 2 × 2 × 2-mm resolution, by using the registration transformations derived as described above. All resulting datasets were concatenated in the temporal dimension, resulting in a 2D dataset with spatial dimension of size 91 × 109 × 91 = 902,629 and 6,226 time points. ICA was run using MELODIC at dimensionalities of 20 and 70. In normal usage, MELODIC estimates the optimal dimensionality of the data; this aids in achieving ICA convergence stability. However, in this case, because we were enforcing the dimensionality and, hence, reducing the likelihood of guaranteed stable convergence, we ran the ICA unmixing 8 times and combined these analyses (via a metalevel ICA decomposition fed by all $d \times 8$ maps) to find the overall most stable decomposition. The ICA spatial maps were Gaussianized as described above. The resulting maps are, at a chosen dimensionality d, the $d - n_{\text{artifacts}}$ most representative resting state covarying networks across a large sample of normal subjects.

Spatial and Functional Associations of the ICA Components. For the 20-component decompositions of the resting FMRI and BrainMap datasets, spatial maps were compared between the 2 sets of results by using simple Pearson correlation of the unthresholded, Gaussianized spatial maps. For the 70-component decompositions, maps were again compared/matched between the resting FMRI and BrainMap results by using spatial correlation, also related to the 20-component decompositions by using a combination of spatial correlations and "functional" correlations (i.e., also by using ICA time courses). This latter analysis is now described in more detail.

Let the matrix of spatial cross-correlation values between the 70-component BrainMap and resting FMRI maps be $R_{\text{S:RSN70}\times\text{BM70}}$. Let the matrix of temporal cross-correlation values between the 70-component BrainMap and 20-component BrainMap maps (where the 20-component maps have been reordered to be consistent between BrainMap and RSNs, according to the pairings found in the 20-component analyses) be $R_{\text{T:BM70}\times\text{BM20}}$, and the matrix of spatial cross-correlations be $R_{\text{S:BM70}\times\text{BM20}}$. Likewise, let the matrices of temporal and spatial correlations from the resting FMRI maps be $R_{\text{T:RSN70}\times\text{RSN20}}$ and $R_{\text{S:RSN70}\times\text{RSN20}}$. When associating 70-component with 20-component maps, we care about both spatial overlap and functional correspondence and so (because these are normalized correlations) average the spatial and temporal matrices to give spatiotemporal correspondence matrices:

$$R_{\text{ST:BM70}\times\text{BM20}} = (R_{\text{S:BM70}\times\text{BM20}} + R_{\text{T:BM70}\times\text{BM20}})/2, \quad \textbf{[s1]}$$

$$R_{\text{ST:RSN70}\times\text{RSN20}} = (R_{\text{S:RSN70}\times\text{RSN20}} + R_{\text{T:RSN70}\times\text{RSN20}})/2. \quad \textbf{[s2]}$$

We now associate 70-component maps with the 20-component maps by combining all of the above spatial and temporal information and utilizing information from both domains simultaneously to give automated pairings across dimensionalities and domains:

$$R_{\text{RSN70}\times\text{BM20}} = R_{\text{S:RSN70}\times\text{BM70}}\, R_{\text{ST:BM70}\times\text{BM20}} \quad \textbf{[s3]}$$

$$R_{\text{RSN70}\times\text{RSN\&BM20}} = R_{\text{RSN70}\times\text{BM20}} \cdot R_{\text{ST:RSN70}\times\text{RSN20}} \quad (\text{Schur product}), \quad \textbf{[s4]}$$

where searches for maxima in the rows of this final matrix, $R_{\text{RSN70}\times\text{RSN\&BM20}}$, map the RSN_{70} maps onto the reordered (and matched) 20-component BrainMap-RSN maps. The equivalent calculation is also made for the BM_{70} maps, resulting in correspondences across dimensionalities and domains.

Extracting Behavioral Domain Information from BrainMap. To add functional interpretation to each of the ICA components, we projected each BrainMap-derived component time course back onto the original list of 7,342 experimental conditions and, hence, extracted the corresponding behavioral domain information from the BrainMap database. We now describe this process in more detail.

We define $e = 7{,}342$ to be the number of "experiments" (different activation conditions in BrainMap) and d to be the dimensionality of the PCA-reduced dataset (e.g., $d = 20$). The standard-brain-space image has $s = 199{,}191$ nonzero voxels. Hence, the raw BrainMap data matrix Y is of size $s \times e$. The PCA decomposition is

$$Y = USV', \quad \textbf{[s5]}$$

where U are the spatial modes, S is a diagonal matrix containing the singular values (ordered, by convention), and V are the "temporal" (experiment ID) modes. To pass on the strongest d spatial modes to the ICA decomposition, we take the first d columns from V (corresponding to the d largest singular values), giving V_{d}, of size $e \times d$, and then calculate

$$U_{\text{d}} = YV_{\text{d}}S_{\text{d}}^{-1}, \quad \textbf{[s6]}$$

which is an $s \times d$ matrix of the top d whitened spatial modes. ICA is then applied, and the resulting mixing matrix M_{d} is of size $d \times d$; to project this back onto the experiment-ID domain, and hence onto BrainMap, we need to reuse V_{d}:

$$M = V_{\text{d}}M_{\text{d}}. \quad \textbf{[s7]}$$

Thus, we have M, an $e \times d$ matrix whose d columns (one for each ICA component) describe the weightings of each component for each of the original activation images. We then extract the b (behavioral domains) $\times$ e matrix P from BrainMap and form the final matrix of domains vs. ICA maps,

$$P_{\text{d}} = PM. \quad \textbf{[s8]}$$

We scale each row of P_{d} to have mean of unity, to normalize for different numbers of different behavioral domains existing in the database. This results in the mapping matrix as seen in Fig. 2 in the main article.

Note that a normalization for the different numbers of different paradigms (behavioral domains) is not straightforward to apply to the raw data fed into the PCA/ICA decomposition, because there will be some functional covariance between the different "paradigms," so it would not be correct to treat every behavioral domain in the same way (in terms of variance scaling); however, it would be good to achieve normalization if possible, to improve the "objectivity" of the derived maps. With respect to the "reverse inference" of ICA spatial maps and experimental-ID-time courses back onto the 66 BrainMap behavioral domains, we note the warning made in articles such as ref. 11; this discusses the danger of oversimplistically assigning a limited set of functions to an "activated" brain region, on the basis of prior experiments that activated that region. Our figure is included for illustrative purposes, and as a "sanity check" for our spatiotemporal manipulations of the BrainMap data; the fact that we have presented the back-projection matrix unthresholded directly relates to the wish for caution in such reverse inference of function from location. In fact, we could immediately head toward the (Bayesian) selectivity discussed by Poldrack if we were to normalize vertically in the matrix, and not just horizontally, as described above.

Results: 20-Dimensional Results in Detail. In this section, we show more complete images of the 10 main corresponding pairs

presented in Fig. 1 of the main article as well as for all other components extracted by the 20-dimensional ICA decompositions of BrainMap and the resting FMRI data. We also give more detailed descriptions of the nonpaired components.

The 10 well-matched pairs of components (maps 1–10_{20}) are shown in Figs. S1 and S2. As with all images in this article, the left side of the brain is shown on the right of the image. All ICA spatial maps were originally Gaussianized via a normalized mixture-model fit, and then thresholded at $Z = 2$ for all images shown in this section. Both datasets are in $2 \times 2 \times 2$-mm MNI152 standard space; every third slice is shown here, starting with the lowest slice at -28 mm in the MNI152 coordinate system.

The weakest spatial correlation in these 10 paired maps is $r = 0.25$ (Pearson). A correction for the number of possible paired comparisons would be a factor of $20 \times 20 = 400$ (conservative because not all components are considered to be nonartifactual). A correction for the spatial degrees of freedom is given via Gaussian random field theory and empirical smoothness estimation (12, 13); for this data, the number of independent "resels" (resolution elements) was found to be ≈665; we therefore set this conservatively to be 500. Applying Fisher's r-to-z transform by using degrees-of-freedom 500, converting to a P value and multiplying by 400 to correct for multiple comparisons, we obtain $P = 5 \times 10^{-6}$, hence, our statement in the main article that the weakest pairing corresponds to (at least as small as) $P = 10^{-5}$ (corrected).

Figs. S3–S5 show BrainMap and RSN components that are plausible functional networks but that did not find a strong and unambiguous (1:1) mapping between BrainMap and the resting FMRI data. Each also has some overlap with the 10 main paired maps, or some combination of these. We have loosely grouped these maps along with one or more of the paired maps (the latter being shown in the top part of each of these 3 figures, for reference), partly on the basis of spatial overlap but also taking into account "functional correspondence." For an RSN, this means using the temporal correlation between the RSN map in question and the paired RSN maps; for a BrainMap map, this means using the experiment-ID correlation between the BrainMap map in question and the paired BrainMap maps.

Fig. S3 shows map BM-11_{20}. This component has clear spatial overlap with the visual subset of paired components, as well as functional similarity to the visual subset of BrainMap components. This map includes the parahippocampal gyrus, lateral occipital cortex, and, possibly, lingual gyrus and primary visual cortices.

Fig. S4 shows map BM-12_{20}. This component has clear spatial overlap with the "default mode network" map 4_{20} as well as functional similarity to the BrainMap 4_{20} map.

Fig. S5 shows maps RSN-11, 12, 13_{20} and BM-13, 14, 15_{20} from the 20-component ICA decomposition of BrainMap and the resting FMRI data. These components do not directly match single maps but do have some spatial overlap with the set of maps 6, 8, 9, 10_{20} as well as functional similarity.

Fig. S6 shows maps RSN-14, 15, 16_{20} and BM-16, 17, 18_{20} from the 20-component ICA decomposition of BrainMap and the resting FMRI data. It is not clear whether the resting FMRI maps are artifactual (e.g., caused by the presence of larger blood vessels), or valid RSNs. The BrainMap maps are biologically plausible, corresponding probably to thalamus/caudate, hippocampus/amygdala, and orbitofrontal cortex/anterior insular; however, the decomposition at this dimensionality did not find exactly corresponding maps in the resting FMRI data.

Fig. S7 shows clearly artifactual maps from the 20-component ICA decomposition of BrainMap and the resting FMRI data. The "RSN" maps do not lie within gray matter and are caused by confound factors such as variations in subjects' head sizes (residual after registration to standard space), head motion, and nonneural physiological fluctuations. ICA has been shown to be very effective at separating such artifacts into separate components from plausible functional components (14). The BrainMap components are mathematical artifacts, again not in gray matter, caused by the temporal variance standardization and data demeaning carried out by the PCA-based initial dimensionality reduction.

1. Talairach J, Tournoux P (1988) *Co-Planar Stereotaxic Atlas of the Human Brain* (Thieme, New York).
2. Turkeltaub P, Eden GF, Jones KM, Zeffiro TA (2002) Meta-analysis of the functional neuroanatomy of single-word reading: Method and validation. *NeuroImage* 16(3):765–780.
3. Eickhoff SB, et al. (2009) Coordinate-based activation likelihood estimation meta-analysis of neuroimaging data: A random-effects approach based on empirical estimates of spatial uncertainty. *Hum Brain Mapp*, in press.
4. Beckmann CF, Smith SM (2004) Probabilistic independent component analysis for functional magnetic resonance imaging. *IEEE Trans Med Imag* 23(2):137–152.
5. Smith SM, et al. et al. (2004) Advances in functional and structural MR image analysis and implementation as FSL. *NeuroImage* 23(S1):208–219.
6. Woolrich MW, et al. (2009) Bayesian analysis of neuroimaging data in FSL. *NeuroImage* 45:S173–S186.
7. Jenkinson M, Bannister PR, Brady JM, Smith SM (2002) Improved optimisation for the robust and accurate linear registration and motion correction of brain images. *NeuroImage* 17(2):825–841.
8. Smith SM (2002) Fast robust automated brain extraction. *Hum Brain Mapp* 17(3):143–155.
9. Andersson J, Smith S, Jenkinson M (2007) Non-linear optimisation. *Internal Technical Report TR07JA1, Oxford Centre for Functional Magnetic Resonance Imaging of the Brain, Department of Clinical Neurology* (Oxford Univ, Oxford, UK), available at www.fmrib.ox.ac.uk/analysis/techrep.
10. Andersson J, Jenkinson M, Smith S (2007) Non-linear registration aka spatial normalisation. *Internal Technical Report TR07JA2, Oxford Centre for Functional Magnetic Resonance Imaging of the Brain, Department of Clinical Neurology* (Oxford Univ, Oxford, UK), available at www.fmrib.ox.ac.uk/analysis/techrep.
11. Poldrack R (2006) Can cognitive processes be inferred from neuroimaging data? *Trends Cognit Sci* 10(2):59–63.
12. Jenkinson M (2000) Estimation of smoothness from the residual field. *Internal Technical Report TR00MJ3, Oxford Centre for Functional Magnetic Resonance Imaging of the Brain, Department of Clinical Neurology* (Oxford Univ, Oxford, UK).
13. Forman S, et al. (1995) Improved assessment of significant activation in functional magnetic resonance imaging (fMRI): Use of a cluster-size threshold. *Magn Reson Med* 33:636–647.
14. Birn R, Murphy K, Bandettini P (2008) The effect of respiration variations on independent component analysis results of resting state connectivity. *Hum Brain Mapp* 29:740–750.

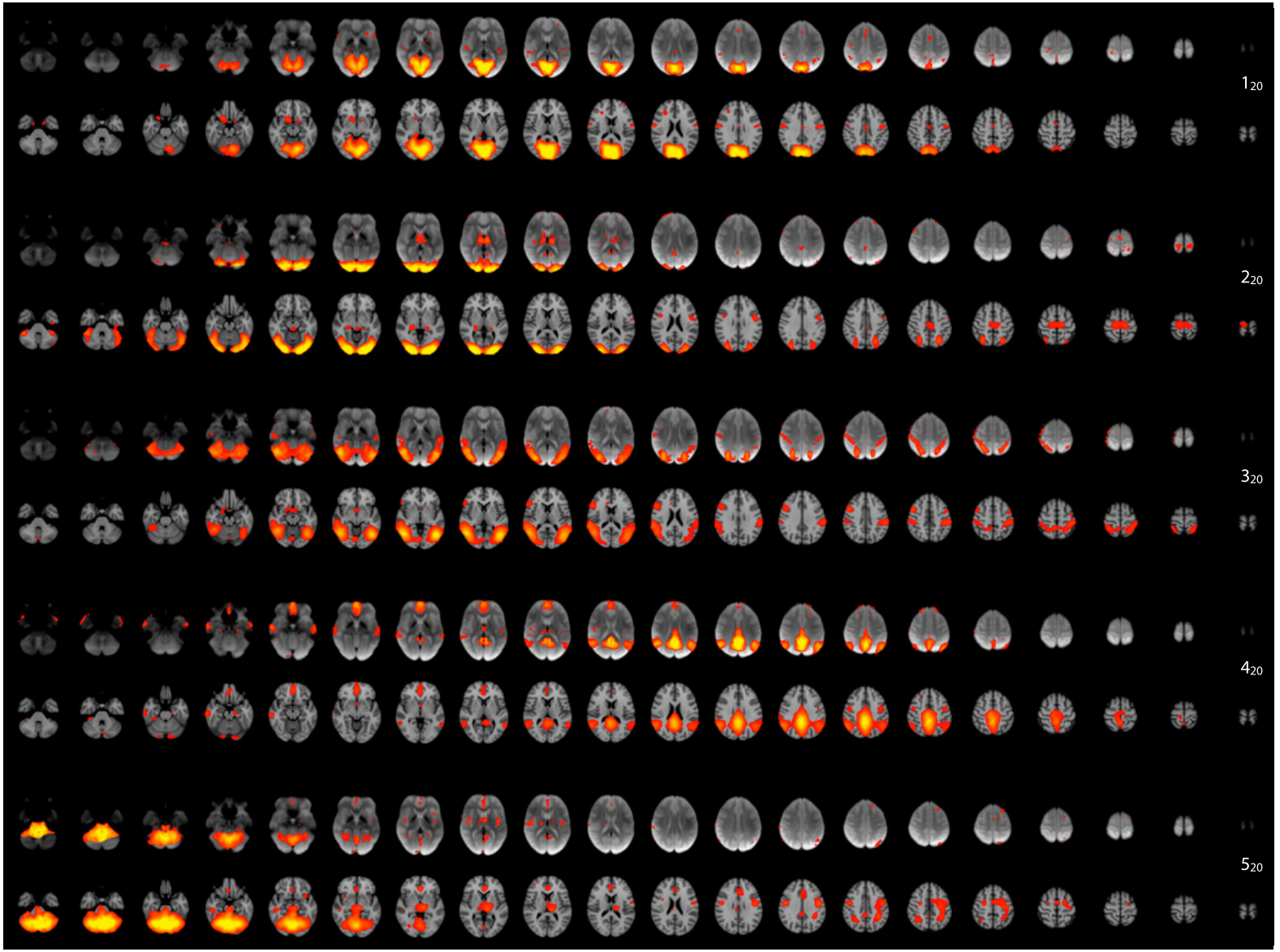

Fig. S1. Maps 1_{20} through 5_{20} of the 10 well-matched pairs of networks from the 20-component ICA decomposition of BrainMap and the resting FMRI data. The top row of each pair is the RSN, and the bottom is the BrainMap network. This figure shows every 3rd axial slice in 2-mm MNI152 standard space, starting with the lowest slice at −28 mm.

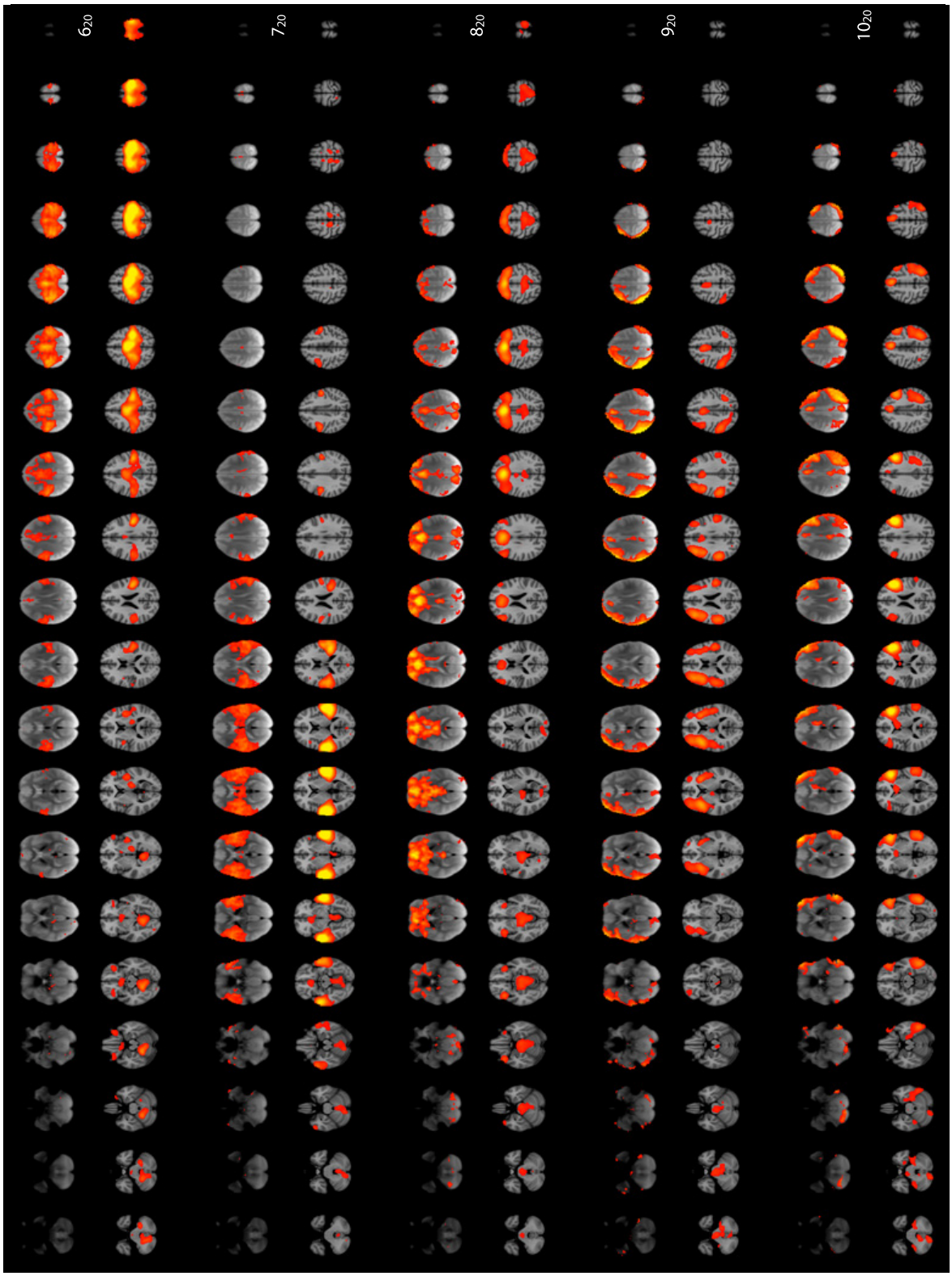

Fig. S2. Maps 6_{20} through 10_{20} of the 10 well-matched pairs of networks from the 20-component ICA decomposition of BrainMap and the resting FMRI data.

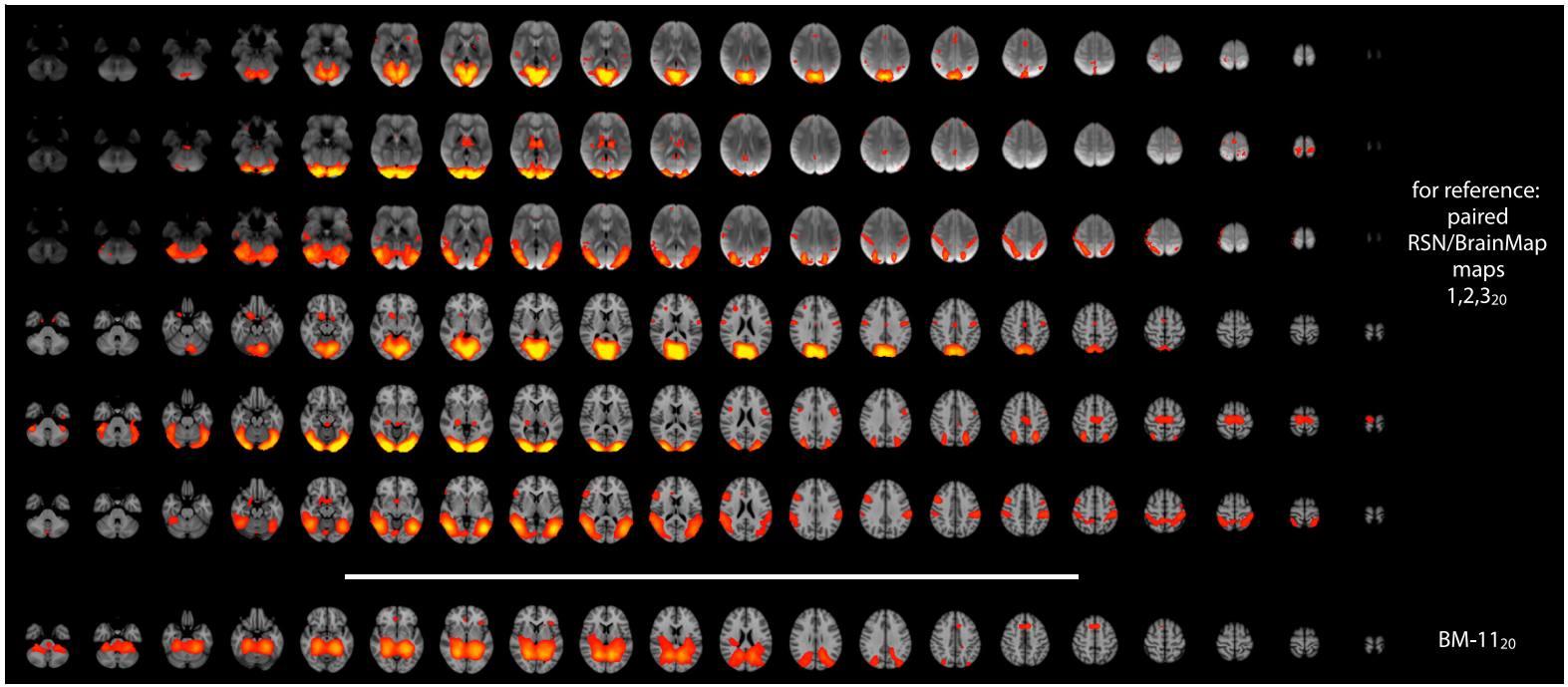

Fig. S3. Map BM-11$_{20}$ from the 20-component ICA decomposition of BrainMap and the resting FMRI data. This component does not directly match a single map from the resting FMRI data but does have spatial overlap with the visual subset of paired components as well as functional similarity to the visual subset of BrainMap components.

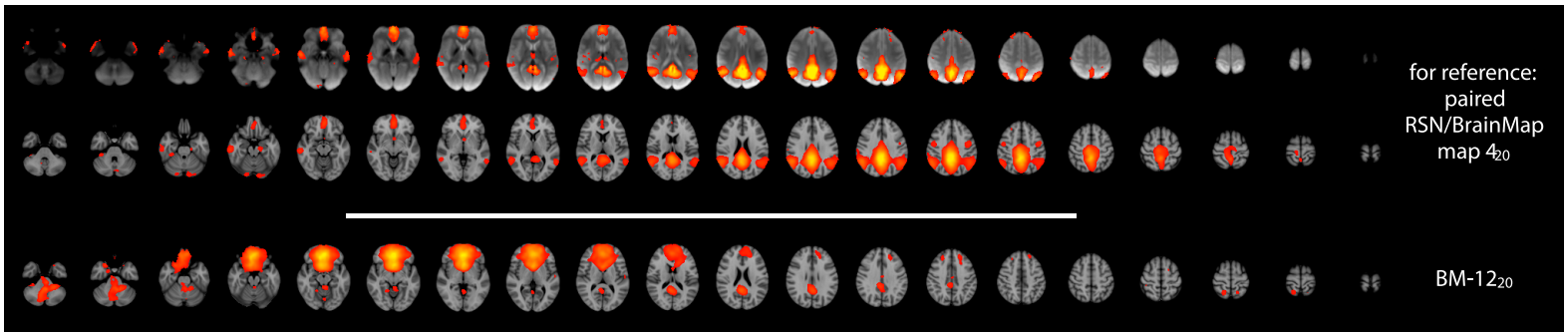

Fig. S4. Map BM-12_{20} from the 20-component ICA decomposition of BrainMap and the resting FMRI data. This component does not directly match a single map from the resting FMRI data but does have clear spatial overlap with the ''default mode network'' map 4_{20} as well as functional similarity (according to the experiment-ID ICA time courses) to the BrainMap 4_{20} map.

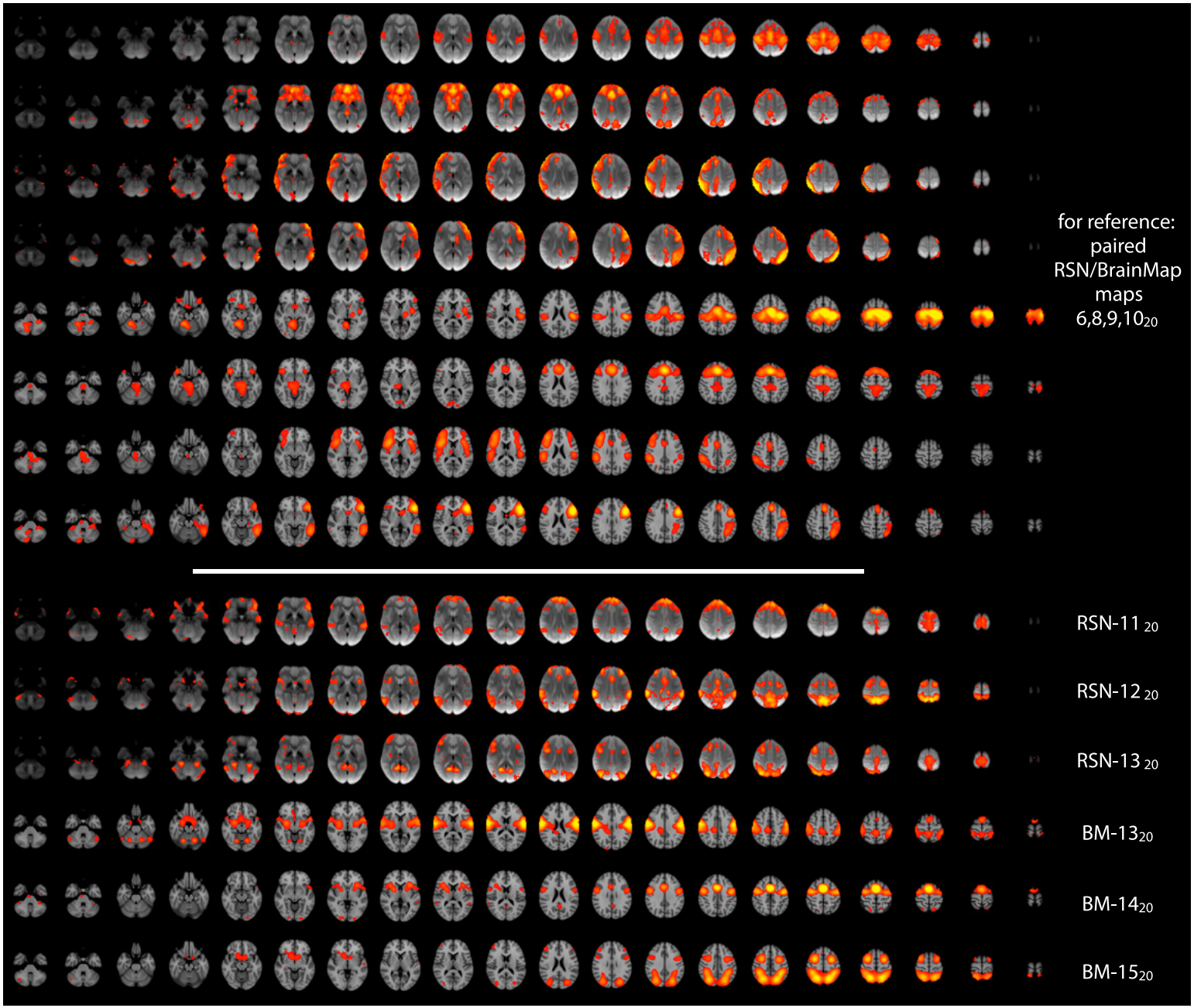

Fig. S5. Maps RSN-11, 12, 13$_{20}$ and BM-13, 14, 15$_{20}$ from the 20-component ICA decomposition of BrainMap and the resting FMRI data. These components do not directly match single maps but do have some spatial overlap with the set of maps 6, 8, 9, 10$_{20}$ as well as functional similarity.

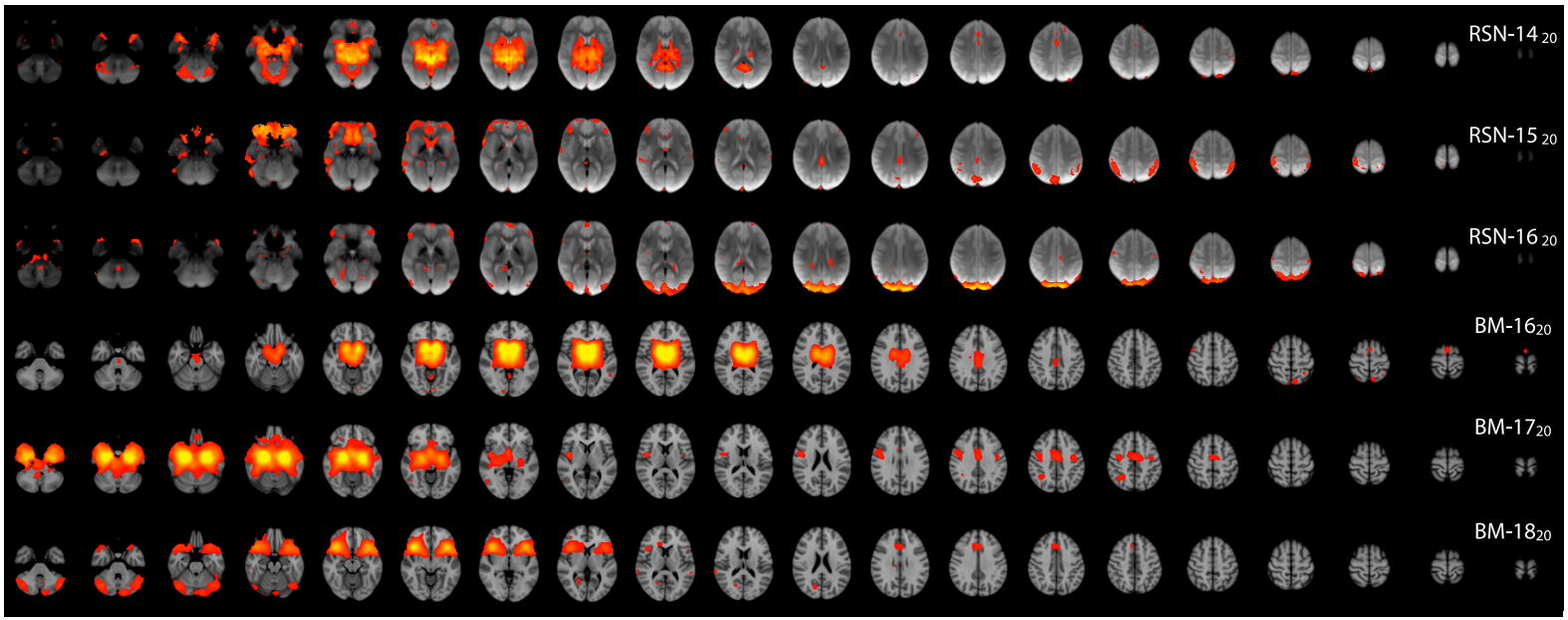

Fig. S6. Maps RSN-14, 15, 16_{20} and BM-16, 17, 18_{20} from the 20-component ICA decomposition of BrainMap and the resting FMRI data. It is not clear whether the resting FMRI maps are artifactual (e.g., caused by the presence of larger blood vessels), or valid RSNs. The BrainMap maps are biologically plausible, corresponding probably to thalamus/caudate, hippocampus/amygdala, and orbitofrontal cortex/anterior insular; however, the decomposition at this dimensionality did not find exactly corresponding maps in the resting FMRI data.

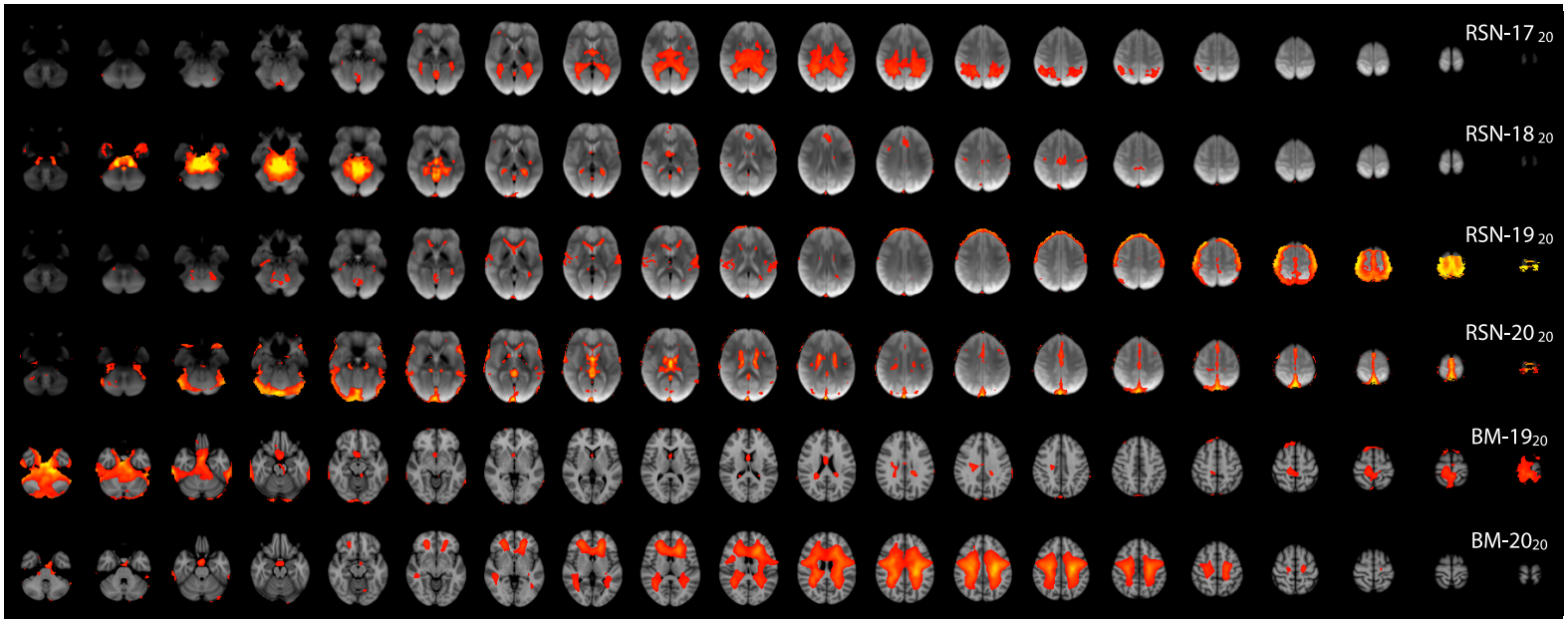

Fig. S7. Clearly artifactual maps from the 20-component ICA decomposition of BrainMap and the resting FMRI data. The ''RSN'' maps are clearly not lying within gray matter and are caused by confounding factors such as variations in subjects' head sizes (residual after registration to standard space), head motion, and nonneural physiological fluctuations. The BrainMap maps are mathematical artifacts, again not in gray matter, caused by the temporal variance standardization and data demeaning carried out by the PCA-based initial dimensionality reduction.